Journal of Physics: Conference Series **551** (2014) 012040 doi:10.1088/1742-6596/551/1/012040

# Paramagnetic muon states in mesoporous carbon materials

**R M Macrae[1], C Upchurch[1], D K Rose[1], Y Miyake[2,3], A Koda[2,3], J S Lord[4], P S Shuttleworth[5,6]**

[1] School of Mathematics and Sciences, Marian University, 3200 Cold Spring Road, Indianapolis, IN 46222, USA
[2] Muon Science Section, Materials and Life Science Division, J-PARC Center, 2-4 Shirane, Shirakata, Tokai-mura, Naka-gun, Ibaraki 319-1195, Japan
[3] Institute of Materials Structure Science, KEK, Tsukuba, Ibaraki 305-0801, Japan
[4] ISIS Facility, Rutherford Appleton Laboratory, Chilton, Oxfordshire, OX11 0QX, UK
[5] Green Chemistry Centre of Excellence, Department of Chemistry, University of York, York YO10 5DD, UK

E-mail: rmacrae@marian.edu

**Abstract.** We present results of longitudinal field repolarisation measurements carried out at J-PARC and ISIS on the "green" functional carbon materials Starbon 300 and Starbon 800, synthesized using starch as a template and subjected to pyrolysis treatments at different temperatures (300°C and 800°C respectively); pyrolysis at low temperature may be expected to yield a material retaining more of the "hydrophilic" properties of the original starch material in its chemically active voids, while high temperature pyrolysis may be expected to lead to "hydrophobic" voids and a more graphitic material. The hydrophilic material shows a larger repolarising fraction than the hydrophobic material, with a hyperfine constant on the order of 200-300 MHz. This is likely to be a superposition of the repolarisation of multiple radicals. Several candidate and model species are investigated through accompanying density functional theory calculations.

## 1. Introduction

Given the approaching world bottlenecks in energy and material resources, interest has recently taken hold in the idea of using carbon biomass as feedstock for the production of low-cost, "green" functional carbon materials. Approaches such as silica-templating [1] and hydrothermal carbonization (HTC) [2] are effective in the morphology-controlled synthesis of carbonaceous nanostructures from carbohydrate parent materials such as starch, cellulose, cyclodextrins, and simple sugars. Such materials are expected to find a variety of technological uses ranging from nanoengineering [3] to spintronics [4] to ultracapacitors [5]. In the last of these, where the storage capacity of electrical double-layer capacitors can be optimized through the use of a nanostructured material, there has recently been interest in replacing activated charcoal (a granular form of carbon in which the interparticle voids constitute the storage space) with better-characterized high-tech forms of carbon such as aligned single-walled nanotubes [6]. Fundamental studies of such materials using a probe which can give some local insight into

[6] Present Address: Polymer Physics Group, CSIC, Madrid, 28006, Spain

the physical and chemical properties of the voids and of the bulk material itself are thus of some importance.

Muon spin rotation studies have been carried out on diamond [7, 8], graphite [9, 10, 11], amorphous carbon [12], fullerenes [13], and nanotubes [14], and are summarized in the recent review by Cox [15]. While in diamond both bond-centered muonium and interstitial muonium are observed [7], in graphite the paramagnetic state formed on muon implantation undergoes rapid spin or charge exchange with the conduction electrons leading to a collapse of the radical line and a temperature-dependent "paramagnetic shift" in the muon Larmor frequency [9, 10, 11]. Insulating amorphous carbon presumably contains a large variety of paramagnetic sites (not experimentally resolvable), but was observed by Cox and Davis to have a diamagnetic fraction of around 40% [12]. In single-walled nanotubes MacFarlane and co-workers observed a high fraction (about 40%) of vacuum-like muonium [14]. Fullerenes show distinct states corresponding to muons stopping respectively inside and outside the cages [13].

Thus, it is evident that $\mu$SR methods distinguish clearly between a variety of different bonding types exhibited by forms of pure carbon; however, to date there have been no studies in the published literature of muon implantation in nanostructured carbonaceous materials of catalytic importance.

## 2. Starbons

Activated carbons are carbonaceous materials with broad industrial applications ranging from biomedical filtration devices to supercapacitors. Typical activated carbons are made using high-temperature inert atmosphere pyrolysis of a hydrocarbon starting material to form a *char*, followed by *activation* via high temperature reaction with $O_2$, $CO_2$, or steam. The meso/microporosity of the material (up to about 500 $m^2/g$ internal pore surface area) is generated by the activation process. The degree of control over the pore structure of the material is typically low.

Recently an alternative strategy for preparation of activated carbon materials has been developed, based on the use of expanded starch as a templating material and relatively mild pyrolysis conditions, with no separate activation step [16]. Properties of these Starbon® materials are "tunable" in a manner dependent on the temperature and duration of pyrolysis; pyrolysis at low temperature may be expected to yield a material retaining more of the "hydrophilic" properties of the original starch material in its chemically active voids, while high temperature pyrolysis may be expected to lead to "hydrophobic" voids and a more graphitic material. Two samples were obtained from the Green Chemistry Centre of Excellence at the University of York, representing the hydrophilic (Starbon 300) and hydrophobic (Starbon 800) extremes of the preparation method. (The numerical suffixes represent the pyrolysis temperature in degrees Celsius.)

## 3. Experimental

Complex amorphous materials are not amenable to study using muon spectroscopy methods that rely upon precise measurement of spin precession frequencies or detection of sharp RF or level crossing resonances, as the spin polarisation is likely to be distributed over a broad variety of muon addition sites; we therefore employed the bluntest instrument in the $\mu$SR arsenal, longitudinal field muon spin repolarisation spectroscopy (LF$\mu$SR). In this method, paramagnetic species are detected via the recovery of muon spin polarisation against an applied longitudinal field, yielding semiquantitative information on the magnitude of the isotropic hyperfine coupling $A_\mu$ (which can distinguish between muonium, high-coupling radicals, or low-coupling radicals), the presence and type of hyperfine anisotropy (axial or complete), and the presence or otherwise of sources of spin relaxation (electron mobility, chemical reactions).

### *3.1. J-PARC measurements*

Room temperature longitudinal field repolarisation measurements were carried out on foil-encapsulated powder samples using the D1 instrument at J-PARC over the field range 0-1600 G; the results appear in Figures 1 (Starbon 300) and 2 (Starbon 800). In Starbon 800 (Figure 2) only a small fraction exhibits repolarisation, while there is a much larger repolarising fraction in Starbon 300. This suggests that the "hydrophilic" material retains substantial isolated radical-forming double bond character whereas the "hydrophobic" material is substantially graphitized. Relaxation rates are modest ($\lambda < 0.5\mu s^{-1}$) over the entire field range.

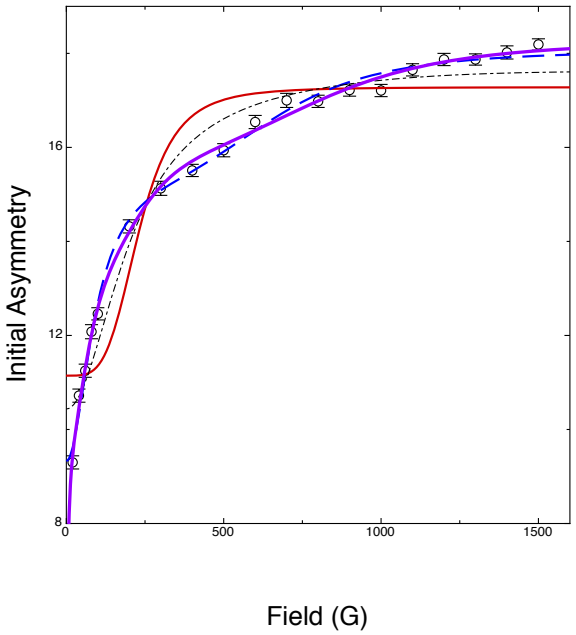


**Figure 1.** Room temperature LF repolarisation curve for Starbon 300. The curves represent fits to the data described in the text.

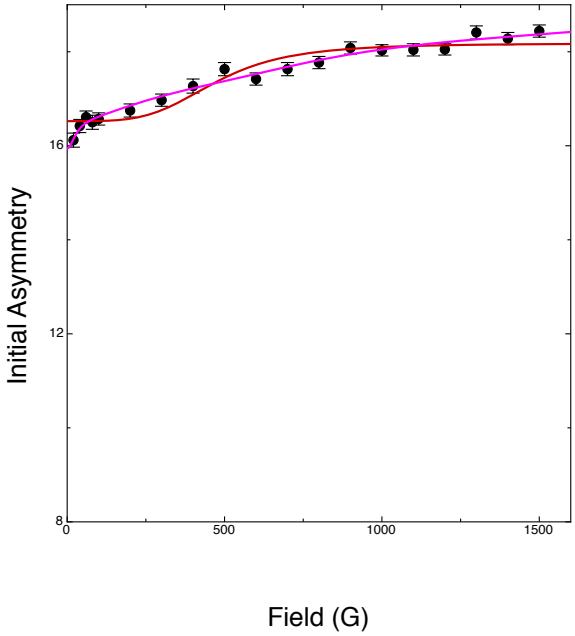


**Figure 2.** Room temperature LF repolarisation curve for Starbon 800. The curves represent fits to the data described in the text.

The solid and dashed curves in Figures 1 and 2 represent fits to the data. One or more repolarising paramagnetic fractions are considered, together with a non-repolarising background. In the hydrophilic sample (Figure 1), a single isotropic radical (solid red curve, $\chi^2 = 12.00$) yields a poor fit to the experimental points, with an optimum $A_\mu$ of 375 MHz. Better fits are obtained by allowing for an anisotropic hyperfine tensor or for more than one radical. A fit to two isotropic radicals yielded a much improved fit (dashed blue curve, $\chi^2 = 0.69$), corresponding to $A_\mu$ values of 258 MHz and 154 MHz. Together, these account for almost all of the observed asymmetry, which is inconsistent with the approximately 1/3 of the total asymmetry observed to precess under transverse field. (This is most likely due to muons stopping in the sample holder; studies with a holmium sample offering the same cross-sectional area as the Starbon sample showed that about 2/3 of the polarisation should be attributed to muons stopping in the sample.) A more appropriate fitting function for a polycrystalline or amorphous solid would make use of one or more radicals with a powder-averaged fully anisotropic hyperfine interaction [18]. With a single repolarising radical fraction in which both the isotropic component and the dipolar part (considered axial) are left as free parameters, the best fit yielded $A_\mu = 574$ MHz and $D_\parallel = 112$ MHz (black dot-dashed curve, $\chi^2 = 4.47$), with the paramagnetic fraction accounting for about 1/3 of the total asymmetry; the fractional hyperfine anisotropy in this fit is somewhat too large to be plausible for a typical muonium adducts to a C=C double bond. Choosing instead to

restrict the anisotropic term to 10% of the magnitude of the isotropic term, but allowing two radicals, yielded $A_\mu$ = 228 MHz (54%) and $A_\mu$ = 298 MHz (24%) (purple curve, $\chi^2$ = 0.43); this approach gave the best quantitative fit, but a slightly larger estimated total asymmetry. (Note that the polarisation recovery is not quite completed at 1600 G in this case.) The red and violet curves in Figure 2 represent isotropic single radical and anisotropic two-radical fits to the Starbon 800 data; the small fraction of recovering polarisation makes reliable fits problematic in this case, but the patterns are consistent with a coupling of some few hundred MHz.

*3.2. ISIS measurements*

As a check on the high-field component of the polarisation recovery, and to search for any level crossings that may be detectable, additional repolarisation scans were carried out on the Starbon 300 sample using the Hi-Fi instrument at ISIS, over a field range up to about 10 kG at 300 K, and up to 5 kG at 20 K. The powder samples were mounted in an Al foil packet, masked with a silver plate. Thus, some part of the non-repolarising fraction probably corresponds to muons stopping in silver. A field scan up to 12 kG was also carried out using an Al foil dummy sample of equivalent stopping density in order to correct for field-dependent background due to changing decay positron trajectories. No sign of any level crossings was seen at fields up to 10 kG, excluding the detection of well-defined zero-crossings from radicals with $A_{\rm iso}$ up to 300 MHz. Fits to the data between 50 G and 5 kG are shown in Figure 3. The repolarisation behavior changes very little between 300 K (solid dots) and 20 K (dots inside circles), indicating that the formation of the paramagnetic species either has a low barrier or is non-thermal, and also that the radicals are likely to be in a rather rigid environment, not strongly subject to dynamical averaging of $A_{\rm iso}$ itself. (That there may be some dynamical modulation of the dipolar part of the coupling is evident from the differences observable at low field.) The fit parameters in each case represent two radicals, each with $D_\parallel$ fixed to $0.1A_\mu$. A relaxing signal component with $\lambda$ on the order of 3 $\mu s^{-1}$ is decoupled in a few tens of gauss. Observed relaxation effects are most likely related to slow desorption of oxygen and other gases from these microporous materials.

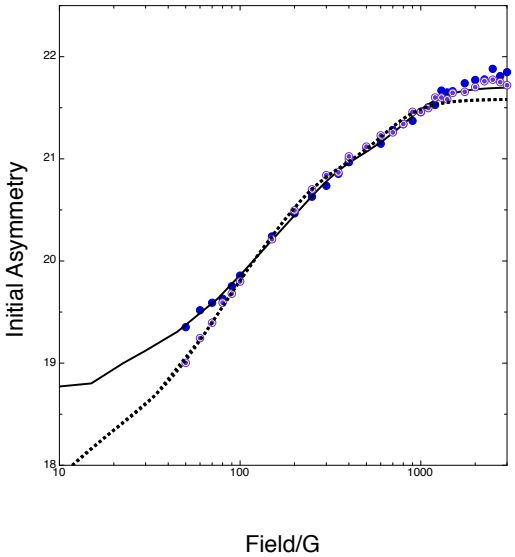


**Figure 3.** LF repolarisation data obtained at 300 K (solid circles, bold solid curve) and 20 K (dots inside circles, bold dotted curve) on the Starbon 300 sample using the Hi-Fi instrument at ISIS. Curves are fits to two anisotropic radials as described above.

Fit parameters:
$A_\mu$ = 297 MHz (14 %) and 178 MHz (6 %), $\chi^2$ = 0.569 (300 K data); $A_\mu$ = 212 MHz (21 %) and 203 MHz (6 %), $\chi^2$ = 0.655 (20 K data).

Simulations using *Quantum* [17] suggest that an alternative model might be a single radical with $A_\mu \sim$ 300 MHz with the low-field part of the polarization recovery then due to decoupling of a *geminal* proton (for which $A_H$ can be expected to be close to $A_\mu/3.1833$); in this case, the difference between the 300 K and 20 K datasets would be due to a change in the thermally-

averaged dipolar part of the hyperfine interaction. Such a picture, however, requires the room temperature hyperfine tensor to be close to isotropic.

## 4. Computational results

Starbons and similar materials are likely to have a complex structure intermediate between that of their parent material (usually starch or cellulose) and graphitic carbon. Thus, there is probably no single dominant type of radical-forming site present in these materials. Nonetheless, it is possible to obtain some information about likely site chemistry from a study of site energetics and the magnitudes of hyperfine coupling constants.

### *4.1. Muonium adducts to hydroxymethylfurfural*

Hydroxymethylfurfural (HMF) is a compound produced in the dehydration of hexose sugars, recently reviewed for its potential as a potential renewable "platform chemical", a starting material in industrial synthesis of polymers, pharmaceuticals, and other products [19]. It has been suggested by Titirici *et al.* as a small-molecule intermediate in the HTC process [20]. Under conditions of reasonably low temperature (below about 300°C), hydrolysis of the starch or cellulose template is followed by dehydration of hexoses into HMF (and of pentoses into furfural), whereupon a complex series of ring-openings, condensations, and aromatisation reactions leads to the final product, a polymeric furanic structure with aliphatic bridges and terminal carbonyl and hydroxyl groups.

All calculations used the computational package *Gaussian 09* [21], at the B3LYP/6-311G(d,p) level of density functional theory. Optimized geometries of the six radical adducts considered are shown in Figure 4, while their relative energies and the corresponding Fermi contact hyperfine couplings (proton values scaled by $\frac{\mu_\mu}{\mu_p}$) appear in Table 1. As Mu addition to C=C is typically more rapid than to C=O, radical 2 may be a reasonable model species for the repolarising fraction in Starbon 300. (Computational studies of more realistic oligomeric models are in progress.)

**Table 1.** Hyperfine coupling constants for muonium adducts to hydroxymethylfurfural calculated as described in the text. No corrections are made for zero-point stretching or vibrational averaging. Pairs of $A_\mu$ values correspond to situations where Mu can add in either of two, slightly inequivalent, ways.

| Radical | Energy/kJ mol$^{-1}$ | $A_\mu$/MHz |
|---|---|---|
| 1 | 0 | -25 |
| 2 | 1.29 | 369/442 |
| 3 | 24.85 | 312 |
| 4 | 43.36 | 318/324 |
| 5 | 79.14 | 251 |
| 6 | 99.00 | 356/662 |

### *4.2. Muonium addition to graphitic analogues*

The use of polycyclic aromatic hydrocarbons as molecular analogs of graphite (edge-terminated with hydrogen) is widespread in the theoretical literature. We utilise the molecule tribenzo[adg]coronene ($C_{36}H_{18}$) as a model of an "all-armchair" nanographene. There are six distinct muonium addition sites to this species: three outer edge sites, two "bay" sites, and an interior site. Addition at edge sites is 50-70 kJ mol$^{-1}$ more favorable than addition at interior

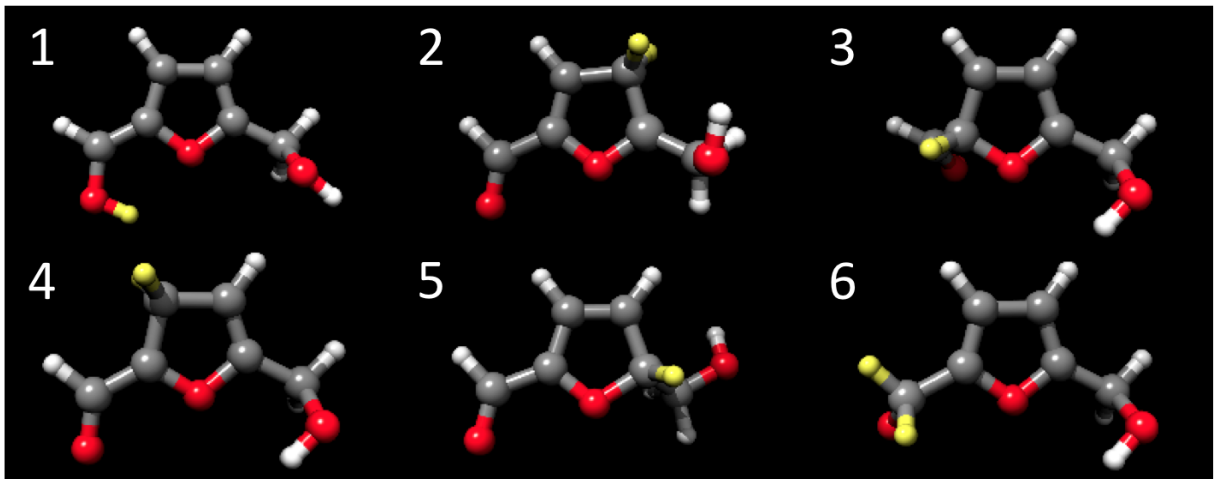


**Figure 4.** Optimized structures of the six muonium adducts to hydroxymethylfurfural. Oxygen atoms are red, carbon atoms grey, hydrogens white. The muon site is indicated in yellow.

or bay sites. Fermi contact couplings for the radicals (scaled to muon values, but uncorrected for the C-Mu zero-point stretch) range from 337 MHz for the lowest-energy edge radical to 583 MHz for the interior radical, which is the least energetically-favorable structure, involving substantial geometrical distortion from the planarity of the parent structure. As an "all-zigzag" model nanographene we consider dibenzo[bc,kl]coronene ($C_{30}H_{14}$), which possesses one terminal site, three edge sites, two "fissure" sites, and three interior sites. In this case the zig-zag edge sites exhibit both the lowest energies overall (lower by about 150 kJ mol$^{-1}$ than the interior or fissure sites), as well as unusually small Fermi contact couplings (down to 80 MHz) occasioned by long-range migration of spin density. A more complete report describing calculations on these species is in preparation and will appear elsewhere.

## Acknowledgments

The authors thank the Green Chemistry Centre of Excellence at the University of York for providing the Starbon samples. The computational part of this work used the Extreme Science and Engineering Discovery Environment (XSEDE), which is supported by National Science Foundation grant number ACI-1053575. The primary computational resource used was the Trestles system at the San Diego Supercomputer Center. PS gratefully acknowledges the Ministerio de Ciencia e Innovación for the concession of a Juan de la Cierva fellowship (JCI-2011-10836). Additionally, RMM and CU thank Marian University for travel support.

## References

[1] Ryoo R, Joo S H and Jun S 1999 *J. Phys. Chem.* B **103** 7743-6
[2] Titirici M-M 2013 *Sustainable Carbon Materials from Hydrothermal Processes* (Chichester: Wiley)
[3] Nakayama N and Akita S 2003 *New J. Phys.* **5** 128
[4] Zhao B, Mönch I, Vinzelberg H, Mühl T and Schneider C M 2002 *Appl. Phys. Lett.* **80** 3144
[5] Stoller M D, Park S, Zhu Y, An J and Ruoff R S 2008 *Nano Lett.* **8** 3498
[6] MIT LEES laboratory project; see e.g `http://lees.mit.edu/lees/posters/RU13_signorelli.pdf`
[7] Holzschuh E, Kündig W, Meier P F, Patterson B D, Sellschop J P F, Stemmet M C and Appel H 1982 *Phys. Rev.* A **25** 1272
[8] Patterson B D 1988 *Rev. Mod. Phys.* **60** 69
[9] Hutchinson D P, Menes J, Shapiro G, Patlach A M and Penman S 1961 *Phys. Rev. Lett.* **7** 129
[10] Chakhalian J, Kiefl R F, Dunsiger S R, MacFarlane W A, Miller R, Sonier J E and Fischer J E 2002 *Phys. Rev.* B **66** 155107

[11] Cox S F J, Cottrell S P, Charlton M, Donnelly P A, Ewels C, Heggie M and Hourahine B 2001 *J. Phys.: Condens. Matter* **13** 2169
[12] Davis E A and Cox S F J 2000 ISIS Annual Report, cited in [15]
[13] Ansaldo E J, Niedermayer C and Stronach C E 1991 *Nature* **353** 121
[14] MacFarlane W A, Chakhalian J, Kiefl R F, Dunsiger S R, Miller R I, Sonier J E, Thess A, Rinzler A G, Smalley R E and Fischer J E 2000 *Physica* B **289-290** 589
[15] Cox S F J 2009 *Rep. Prog. Phys.* **72** 116501
[16] Budarin V, Clark J H, Hardy J J E, Luque R, Milkowski K, Tavener S J and Wilson A J 2006 *Angew. Chem. Int. Ed.* **45** 3782
[17] Lord J S 2006 *Physica* B **374-375** 472-474
[18] Pratt F L 1997 *Phil. Mag. Lett.* **75** 371
[19] van Putten R J, van der Waal J C, de Jong E, Rasrendra C B, Heeres H J and de Vries J G 2013 *Chem. Rev.* **113** 1499-597
[20] Titirici M-M, White R J, Falco C and Sevilla M 2012 *Energy. Environ. Sci.* **5** 6796-822
[21] Gaussian 09, Revision D.01, Frisch M J *et al.*, Gaussian, Inc., Wallingford CT, 2013